Sound & Vibration 2025, 59(5), 2531.
doi: https://doi.org/10.59400/sv2531

Article

Nonlinear vibration of thin-walled box beams incorporating axial displacement, torsion distortion and secondary torsion

Minyao Tan[1], Dequan Guo[1,*], Bo Liu[2], Yu Liu[2]

[1] School of Automation, Chengdu University of Information Technology, Chengdu 610225, China
[2] Sichuan Academy of Agricultural Machinery Science, Chengdu 610066, China
*** Corresponding author:** Dequan Guo, guodq@cuit.edu.cn

CITATION

Tan M, Guo D, Liu B, et al. Nonlinear vibration of thin-walled box beams incorporating axial displacement, torsion distortion and secondary torsion. Sound & Vibration. 2025; 59(5): 2531. https://doi.org/10.59400/sv2531

ARTICLE INFO

Received: 6 June 2025
Revised: 18 August 2025
Accepted: 11 September 2025
Available online: 16 October 2025

Abstract: In this paper, the boundary element method for nonlinear vibration of thin-walled box beams is established, including axial displacement, torsion, distortion, and quadratic torsion. The thin-walled box girders are subjected to conservative dynamic torsional and warping moments that are arbitrarily distributed or concentrated along the length direction. Its control differential equations and boundary conditions are represented by torsion, distortion, and secondary torsional deformation. Its nonlinear terms show strong coupling. The coupling effects of axial displacement, torsion, distortion, and quadratic torsion deformation are fully considered, and the vibration analysis is carried out, respectively, in the state of buckling or post-buckling. The nonlinear differential algebraic equations can be obtained by using the simulation equation method based on the initial boundary value problem, and solved by using an effective time-discrete scheme. In addition, it is proven by two examples that the nonlinear term has a great influence on the torsional moment and the mode of the thin-walled box girder under free vibration. Large torsional rotations increase the torsional stiffness of the thin-walled box beam, ultimately leading to a higher natural frequency. Although the influence of the distortion moment is not as good as that of the torsion moment, it cannot be ignored. The axial inertia term has an obvious influence on the axial stress.

Keywords: thin-walled box beam; nonuniform torsion; distortion; nonlinear; vibration

1. Introduction

In engineering practice, the thin-walled box beams (TBB) are often subjected to eccentric and torsional loads. Meanwhile, due to functional requirements, some stiffening ribs will be arranged inside the TBB or irregular columns. Therefore, it is very important to consider lightweight in the structural design. When the edges or any internal points of TBB are subjected to uneven torsion and distortion, the results of applying elastic analysis may be very conservative due to the significant differences between the initial buckling and complete plasticization of the TBB cross-section that has a large torsional deformation and distortion. It is not enough to merely regard torsional deformation as very small and ignore the influence of the distortion. Therefore, it becomes crucial to study the nonlinear effects of these components. For example, in the finite displacement-small strain theory, the retained nonlinear terms are nonlinearized by the strain-displacement relationship. When torsion and distortion are taken into account, the dynamic analysis of the non-uniform torsion and distortion becomes more complex. It contains the nonlinear coupling of torsion, distortion, and axial displacement balance equations. In this state, it is crucial to analyze the axial load

and boundary conditions and conduct a strict dynamic analysis of the TBB.

The basis for evaluating the moving parts of thin-walled hollow beams is stress analysis under axial and/or bending forces, rather than torsional load. Saint-Venant estimated shear stress using the method of boundary value problems for the first time, and various analytical and numerical methods were employed to conduct extensive analysis and research on it. However, due to the coexistence of tangential stress and warping shear stress, the form of shear stress distribution in the Saint-Venant (principal) theory is no longer applicable in the case of non-uniform torsion. Then, some specialized theories have developed to address non-uniform torsion problems, such as analytical and semi-analytical methods. Among them, the Vlasov theory is the most well-known theory for calculating thin-walled section beams, and a similar second-order beam theory for calculating bending and non-uniform torsion. The above theories are aimed at torsion of open thin-walled structures. Rozmarynowski and Szymczak [1] only analyzed the free torsional vibration of axially immovable thin-walled structures, ignoring some nonlinear terms and the axial inertia term. Without using any static or kinematic assumptions, Ladevèze and Simmonds [2] proposed a stress field-dependent 'exact' beam theory based on a complete three-dimensional function for analyzing beams under arbitrary loads and boundary conditions. In addition to the well-known principal shear stress (Saint-Venant), the beam also generates normal shear stress and secondary shear stress (warping), which are respectively caused by warping (bending moment) and secondary torsional (twisted-torsion) bending moments. At this point, the improved Saint-Venant theory is usually adopted for torsion analysis, and a special mass matrix is used simultaneously. Typically, when the influence of secondary torsional deformation (STMDE) is not considered, bicurvature is selected as the additional warping degree of freedom.

In the book published by ADINA R&D [3], only the warping effect influence is included, but the shear deformation influence is not. Beam elements can be combined with lumped or uniform mass matrices. For general standard beam elements, the uniform mass matrix established by Przemieniecki [4] eliminated the additional terms caused by the warping constant $I\omega$. Based on the displacement formulation of Hermitian and isoparametric three-dimensional beam elements, Bathe and Chaudhary [5] studied the torsional stiffness of rectangular cross-section beams expressed by the warping displacement function. Sapountzakis et al. [6–9] took into account both non-uniform warping and the influence of secondary torsional shear deformation, and used the boundary element method (BEM) to solve the problem of non-uniform torsional vibration with double symmetry and equal cross-section. Considering the influences of geometric nonlinearity, moment of inertia, and warping inertia, the elastic non-uniform torsional dynamics analysis of cylindrical girders with arbitrary cross-sections was carried out within the frame of BEM. Taking into account the nonlinear strain-displacement relationship, Sina et al. [10, 11] studied the axial torsional vibration of the rotating pretwisted thin-walled composite box girder with primary warping and secondary warping. Based on the isogeometric method of Timoshenko beam theory, Lee and Park [12] developed a free vibration analysis of Timoshenko beams with thick beam elements that allow for transverse shear deformation and rotational inertia effects. Stoykov and Ribeiro [13] studied the geometric nonlinear spatial free vibration and forced vibration of asymmetric cross-section

beams in the frequency domain using the P-type finite element method (FEM). The warping function of the beam model was numerically calculated using BEM. Ferradi and Cespedes [14] used a new approach to analyze the lateral deformation and warping of the girder cross-section. That is, the section is decomposed into one-dimensional elements of thin-walled structures and triangular elements of arbitrary cross-sections to determine the lateral deformation mode, and the stiffness matrix is combined to extract feature pairs from it. Yoon et al. [15] applied a geometric nonlinear finite element formula for analyzing three-dimensional beams with functional gradients. This formula adopts beam elements with warping displacement based on continuum mechanics to simulate complex deformation modes. For the first torsional characteristic frequency, the methods proposed in the solid finite element, Stoykov and Ribeiro [13] and Moaveni [16], clearly give the most consistent results. The differences between the results increase for higher-order modes, especially for short beams. The side wall deformation of the beam is included in the high torsional intrinsic mode calculated by the solid finite element method. This effect cannot be considered in a straightforward warping. Murin et al. [17] verified that all the characteristic frequencies of the torsional warping free vibration of the rectangular hollow cross-section beam were in good agreement with the experimental results by considering STMDE.

Numerical solutions of inhomogeneous torsion in recent studies [18–22] have been treated in other recent fields. Finally, Dikaros et al. [23] presented a universal formula for the dynamic analysis of non-uniform warping of beams with any cross-section under any unexpected load and general boundary conditions. The four independent warping parameters are respectively multiplied by one shear warping function and two torsional warping functions in each direction of the three-dimensional coordinate. The accuracy is higher compared with the results of the solid finite element solution. This is because the distortion effect of the cross-section is suppressed in the solid model. A common point of the above-mentioned papers is that the influence of axial force on torsional warping is ignored.

In the recent literature, there is relatively little information on solutions for free and forced torsional vibration of hollow section beams containing non-uniform torsional effects. Sapountzakis and Argyridi [24, 25] proposed a boundary element method (BEM) for solving the non-uniform torsional vibration of an arbitrarily variable cross-section bi-symmetric composite bar. On the basis of geometric nonlinearity, three-dimensional dynamic analysis of the finite boundary beam element was carried out under arbitrary distributed dynamic loads by considering the influence of rotational inertia and warping inertia. Using the equations of the traditional thin plate theory, Balch and Steele [26] established the eigenvalue problem of the effect of self-balancing end loads on thin-walled rectangular section tubes or box girders. In addition to the stress characteristic functions corresponding to the axial warping and lateral deformation of the cross-section, the attenuation distance is of the order of magnitude or shorter than the width of the cross-section. The closed-type solution of thin-walled asymptotically effective in the state of slow attenuation warping or distortion is obtained.

Bosewell and Li [27] considered the coupling relationship between torsional and

distortion warping in the analysis of thin-walled girders. To study the deformation process of thin-walled box beams, Wang [28] simultaneously optimized three conventional methods by using energy variational calculus and static equilibrium methods. Based on the displacement fields of warping, torsion, distortion, and shear lag, Tan et al. [29, 30] established the nonlinear calculation theory of the buckling capacity and free vibration of a straight thin-walled girder. On the basis of the nonlinear motion model of higher-order theory, Saoula and Meftah [31] studied the influence of distortion and shear deformation of TBB elements under axial force and bending force on elastic lateral torsional buckling. Cambronero-Barrientos et al. [32] proposed a beam-type element to address these objectives for thin-wall sections. The unit has three nodes with five degrees of freedom each, instead of the six degrees of freedom of a traditional 3D beam, incorporating both uniform and non-uniform effects of shear hysteresis, torsion, and distortion in the normal stress distribution. Based on the Symplectic method and high-order beam theory, Arici et al. [33] proposed a practical analytical method that overcomes the difficulties of the finite element numerical method. The shear hysteresis effect, distortion, and non-uniform torsion of the curved box girder bridge were analyzed through the Hamiltonian structural analysis method. To analyze the deformation of the cantilever box girder, Li et al. [34] established a one-dimensional fine finite element model considering the non-uniform distortion warping and the secondary distortion, in which the in-plane and out-of-plane deformations of any point around the edge of the cross-section were unified into the same form. Fan and She [35] discussed the transient response characteristics of graphene platelet-reinforced metal foam (GPLRMF) beams with initial geometric defects under pulse loads for the first time. Zhao et al. [36,37] analyzed the vibrations of the laminated quadrilateral plane and the curved plate of the composite material by using FEM, and combined the Jacobi polynomial with the piecewise strategy. Meanwhile, based on the fast multi-pole boundary element integral equation and the regional segmentation mapping as the control equation method of the coupled boundaries, they proposed a coupled Ritz-SEA hybrid method for calculating the constant load and random load of the vibration of the rectangular plate.

This paper studies the dynamic characteristics of a thin-walled box beam, describes the numerical analysis method of the model, and realizes the free vibration analysis by using BEM. In addition, this paper also studies the effect of distortion and non-uniform torsion on moment of inertia terms. The accuracy of this model is verified by reference solutions available in the literature. Then it outlines the characteristics of the current model. Thin-walled box beam support is possible under any boundary conditions, from rigidity to elasticity. The model is original both in analytical and numerical methods.

Here, the main assumptions of the model are as follows:

a) The contour does not deform in its own plane;
b) The distribution of the surface shear strain in the contour direction of the shell wall should follow the Saint-Venant torsion;
c) The Kirchhoff-Love hypothesis is applied to the thin wall.

2. Statement of the problem

2.1. The displacement field

Figure 1 is the global Cartesian coordinate system (x, y, z). Establish the *Syz* coordinate system through the shear center of the cross-section. The local coordinate system is represented by (s, n, x). In each wall, s runs through the centerline of entire cross-section, and n is the coordinate of the local normal line. It is assumed that the stress-strain relationship of TBB is the elastic-plastic strain. The TBB is subjected to arbitrarily concentrated or distributed force $n = n\ (x,\ t)$, a twisting moment $m_t = m_t\ (x,\ t)$ and a warping moment $m_w = m_w\ (x,\ t)$ in the x-axis direction.

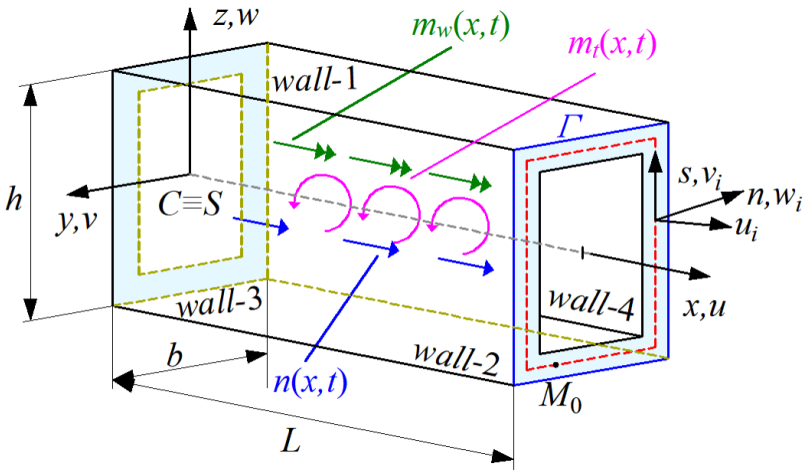

Figure 1. The detailed coordinates of TBB subjected to axial and torsional loading.

The local coordinate system of any point $M_0(s,n,x)$ on the intermediate surface can be represented by the displacements $v(x,s,n,t)$, $w(x,s,n,t)$ and $u(x,s,n,t)$ along the y-, z-,and x- axes. Under the action of the above-mentioned loads, the TBB displacement field considering warping shear stress is set as below [29]:

$$u^i(x,n,s,t) = u_0(x,t) + \phi_s^{Pi}(n,s)\,\theta_x'(x,t) \tag{1a}$$

$$v^i(x,n,s,t) = -h^i(s)\theta_x(x,t) + \eta_s^i(s,n)\,\chi(x,t) \tag{1b}$$

$$w^i(x,n,s,t) = -s\theta_x(x,t) + \phi_s^{\chi i}(s)\chi(x,t) \tag{1c}$$

Where, $i = 1\sim4$ is the number of walls of TBB. $\theta_x(x,t)$ is the torsion angle; $\phi_s^{Pi}(n,s)$ is the primary warping function relative to the shear center S; $\chi(x,t)$ is the distortion angle. According to the beam-frame method, a reasonable displacement field was established by Argyridi and Sapountzakis [25] and Mokos and Sapountzakis [38]. The functions $h^i(s)$, $\phi_s^{\chi i}(s)$ and $\eta^i(s,n)$ in Equation (1) can be expressed as:

$$h^i(s) = \xi_1^i Z^i(s) + \xi_2^i Y^i(s) \tag{2a}$$

$$\eta^i(s,n) = \phi_s^{\chi i}(s) + n\frac{\partial \phi_n^{\chi i}(s)}{\partial s} \tag{2b}$$

$$\phi_s^{\chi i}(s) = \frac{dZ^i(s)}{ds}Y^i(s) - \frac{dY^i(s)}{ds}Z^i(s) \tag{2c}$$

$$Z^i(s) = \xi_1 \frac{h}{2} + \xi_2 s \tag{2d}$$

$$Y^i(s) = \xi_2 \frac{b}{2} + \xi_1 s \tag{2e}$$

$$\phi_n^{\chi i}(s) = \left(-\frac{L_{side}}{2} + \frac{3}{L_{side}}s^2 - \frac{2}{L_{side}^2}s^3\right)(-1)^{i+1}\kappa, \quad \text{with } \kappa = \begin{cases} \frac{2b}{b+h} & i = 1,3 \\ \frac{2h}{b+h} & i = 2,4 \end{cases} \tag{2f}$$

$$\xi_1 = \frac{1+(-1)^{i+1}}{2}(i-2) \tag{2g}$$

$$\xi_2 = \frac{1+(-1)^{i}}{2}(3-i) \tag{2h}$$

Where, *b* is the width of the cross-section, and *h* is height of the cross-section. L represents the entire length of TBB. t_i represents the wall thickness, and each wall thickness is much smaller than the other dimensions. L_{side} represents the variable lengths corresponding to each side of TBB cross-section.

2.2. Stain and stress

By adopting the strain-displacement relationship of 3-D elasticity with moderate displacement, the strain components are shown as follows:

$$\varepsilon_{xx}^i = \frac{\partial u}{\partial x} + \frac{1}{2}\left[\left(\frac{\partial u}{\partial x}\right)^2 + \left(\frac{\partial v}{\partial x}\right)^2 + \left(\frac{\partial w}{\partial x}\right)^2\right] \approx \frac{\partial u}{\partial x} + \frac{1}{2}\left[\left(\frac{\partial \nu}{\partial x}\right)^2 + \left(\frac{\partial w}{\partial x}\right)^2\right] \tag{3a}$$

$$\gamma_{xs}^i = \frac{\partial u}{\partial s} + \frac{\partial \nu}{\partial x} + \frac{\partial u}{\partial x}\frac{\partial u}{\partial s} + \frac{\partial \nu}{\partial x}\frac{\partial \nu}{\partial s} + \frac{\partial w}{\partial x}\frac{\partial w}{\partial s} \approx \frac{\partial u}{\partial s} + \frac{\partial \nu}{\partial x} \tag{3b}$$

$$\gamma_{xn}^i = \frac{\partial u}{\partial n} + \frac{\partial w}{\partial x} + \frac{\partial u}{\partial x}\frac{\partial u}{\partial n} + \frac{\partial \nu}{\partial x}\frac{\partial \nu}{\partial n} + \frac{\partial w}{\partial x}\frac{\partial w}{\partial n} \approx \frac{\partial u}{\partial n} + \frac{\partial w}{\partial x} \tag{3c}$$

For moderate displacements, it can be assumed that some terms have be omitted [36]. To clarify the strain tensor, the longitudinal strain ε_{xx} and shear strains γ_{xs}, γ_{xn} exhibit moderate displacements and include linear strain. Substituting Equation (1) into the well-known 3-D linear strain-displacement relationship, the non-disappearing compatible strain results can be expressed as:

$$\varepsilon_{xx}^i = u_0^{'} + \phi_s^{Pi}\theta_x^{''} + \frac{1}{2}(s^2 + h^2(s))(\theta_x^{'})^2 + \frac{1}{2}((\phi_s^{\chi i})^2 + \eta^2(s,n))(\chi^{'})^2 + (s\eta(s,n) - h(s)\phi_s^{\chi i})\theta_x^{'}\chi^{'} \tag{4a}$$

$$\gamma_{xs}^i = \left(\frac{\partial \phi_s^{Pi}}{\partial s} - h^i(s)\right)\theta_x^{'} + \phi_z^{\chi i}\chi^{'} \tag{4b}$$

$$\gamma_{xn}^i = \left(\frac{\partial \phi_s^{Pi}}{\partial n} + s\right)\theta_s^{'} + \eta^i\chi^{'} \tag{4c}$$

On the basis of Hooke's law, the form of stresses can be easily obtained:

$$\begin{bmatrix} \sigma_{xx} \\ \tau_{xs} \\ \tau_{xn} \end{bmatrix} = \begin{bmatrix} E & & \\ & G & \\ & & G \end{bmatrix} \begin{bmatrix} \varepsilon_{xx} \\ \gamma_{xs} \\ \gamma_{xn} \end{bmatrix} \tag{5}$$

Under the condition of linear elastic behavior, E is the Young's modulus constant and G is shear modulus constant.

2.3. Evaluation of the primary warping function ϕ_s^P

Based on the following boundary value problem, the primary warping function ϕ_s^P can be solved independently [27,28]:

$$\nabla^2 \phi_s^P = 0 \text{ in } \Omega \tag{6a}$$

$$\frac{\partial \phi_s^P}{\partial n} = z n_y - y n_z \text{ on } \Gamma \tag{6b}$$

Where, the Laplace operator is represented by $\nabla^2 = \partial^2/\partial y^2 + \partial^2/\partial z^2$. Ω is a two-dimensional multi-connected region in the y and z planes, and $\partial/\partial n$ represents the directional derivative perpendicular to the boundary Γ. The Neumann type boundary conditions is applicable to the current problem. The obtained warping function to be solved has an integral constant. Therefore, the constant is obtained by introducing the constraints as follow:

$$\int_\Omega \phi_s^P d\Omega = 0 \tag{7}$$

It is noted that the local equilibrium equation solves the torsion problem to the greatest extent in the vertical direction, while any other constraint can be applied. The average axial displacement could be interpreted by Equation (1a) as follow:

$$\int_\Omega u d\Omega = u_0 \cdot A + \theta' \cdot \int_\Omega \phi_s^P d\Omega \tag{8a}$$

$$u_0 = \frac{\int_\Omega u d\Omega}{A} \tag{8b}$$

In which, A represents the cross-sectional area of TBB.

2.4. Equations of global equilibrium

The stress values of TBB can be given naturally:

$$N = \sum_{i=1\sim4} \int_\Omega \sigma_{\varepsilon\varepsilon} d\Omega \tag{9a}$$

$$M_t^P = \sum_{i=1\sim4} \int_\Omega \left[\tau_{xs}^i \left(\frac{\partial \phi_s^{Pi}}{\partial s} - h^i(s) \right) + \tau_{xn}^i \left(\frac{\partial \phi_s^{Pi}}{\partial n} + s \right) \right] d\Omega \tag{9b}$$

$$M_\omega = - \sum_{i=1\sim4} \int_\Omega \varepsilon_{xx} \phi_s^{Pi} d\Omega \tag{9c}$$

$$M_{\Psi}^{\chi} = \sum_{i=1\sim4} \int_{\Omega} [\tau_{xs}\phi_n^{\chi i} + \tau_{xn}\eta^{\chi i}] d\Omega \tag{9d}$$

Where M_t^P represents the primary torsional moment caused by the primary shear stress [11] (the warping shear stress is not considered in the formulation). M_ω represents the warping moment (bi-moment) caused by the torsional curvature. M_{Ψ}^{χ} is the distortion moment. It is worth noting that Equation (9) can also be expressed as:

$$N = EAu_0^{'}(x) + \frac{1}{2}EI_p\theta_x^{'2}(x) + \frac{1}{2}EI_{\chi}\chi^{'2}(x) + EI_{p\chi}\ \theta_x^{'}(x)\chi^{'}(x) \tag{10a}$$

$$M_t^P = GI_t \cdot \theta^{'} \tag{10b}$$

$$M_{\omega} = -EC_s\ \cdot \theta^{''} \tag{10c}$$

$$M_{\Psi}^{\chi} = GI_d \cdot \chi^{''} \tag{10d}$$

Where, I_t is the torsion constant, I_p is the torsion polar moment of inertia, C_s is the warping constant, I_d is the distortion constant, I_χ is the distortion polar moment of inertia and $I_{p\chi}$ is the torsion and distortion coupling constant in regard to the shear center *S.* And its details are as follows:

$$I_p = \sum_{i=1\sim4} \int_{\Omega} \left(h^i(s)^2 + s^2\right) d\Omega \tag{11a}$$

$$I_i = \sum_{i=1\sim4} \int_{\Omega} (h^i(s)^2 + s^2 + s \cdot \frac{\partial \phi_s^{Pi}}{\partial n} - n \cdot \frac{\partial \phi_s^{Pi}}{\partial s}) d\Omega \tag{11b}$$

$$C_s = \sum_{i=1\sim4} \int_{\Omega} (\partial \phi_s^{Pi})^2 d\Omega \tag{11c}$$

$$I_d = \int_{\Omega} (\phi_z^{\chi} \frac{\partial \phi_s^{Pi}}{\partial s} + \eta \frac{\partial \phi_s^{Pi}}{\partial n}) d\Omega \tag{11d}$$

$$I_{\chi} = \int_{\Omega} \left(\eta_s^{i2} + \phi_s^{\chi i2}\right) d\Omega \tag{11e}$$

$$I_{p\chi} = \int_{\Omega} \left(s\eta_s^i + h\phi_s^{\chi i}\right)^2 d\Omega \tag{11f}$$

Significantly, the above stress resultants are due to the cross-section direction of their deformation forms (including the rotation of the cross-section), as they are defined according to Equation 10(b–d) and have been shown to be the same as the direction in the linear case.

For establishing global equilibrium equations, the virtual work principle is adopted to express it as:

$$\delta W_{int} + \delta W_{mass} = \delta W_{ext} \tag{12}$$

Where:

$$\delta W_{\text{int}} = \int_V (\sigma_{xx}\delta\varepsilon_{xx} + \tau_{xs}\delta\gamma_{xs} + \tau_{xn}\delta\gamma_{xn})dV \tag{12a}$$

$$\delta W_{mass} = \int_V \rho \cdot (\ddot{u}\delta u + \ddot{\nu}\delta\nu + \ddot{w}\delta w)dV \tag{12b}$$

$$\delta W_{ext} = \int_F (t_x\,\delta u\ + t_s\,\delta\nu + t_n\,\delta w)\,dF \tag{12c}$$

Where, $\delta(\cdot)$ represents virtual quantities. ρ represents density. $(\cdot)$ represents the differential with respect to time. V, F are the volume and cross-section of TBB, respectively. t_x, t_y, t_z are the components of the fractional vector with respect to the surface of the box girder that has not deformed.

Substitute the strain components in Equation (4) and the displacement components in Equations (1)–(12), and obtain the governing partial differential equations of TBB through algebraic calculation:

$$\rho A\ddot{u} - \frac{\partial N}{\partial x} = n(x,t) \tag{13a}$$

$$\begin{aligned}&\rho I_p\ddot{\theta}_x + \rho C_s\ddot{\theta}_s'' - \frac{\partial M_t^P}{\partial x} - \frac{\partial^2 M_\omega}{\partial x^2} - \frac{3}{2}EI_{pp}(\theta_x')^2\theta_x'' - EI_p u'\theta_x'' - EI_p u''\theta_x' - EI_{p\chi}\theta_x''\chi' - EI_{p\chi}\theta_x'\chi' \\ &= m_t(x,t) + \frac{\partial m_\omega(x,t)}{\partial x}\end{aligned} \tag{13b}$$

$$\rho I_\chi\ddot{\chi} - \frac{\partial M_t^\chi}{\partial x} - \frac{3}{2}EI_{\chi\chi}(\chi')^2\chi'' - EI_\chi u'\chi'' - EI_\chi u''\chi' - EI_{p\chi}\chi''\theta_\chi' - EI_{p\chi}\chi'\theta_\chi'' = m_\chi(x,t) \tag{13c}$$

The corresponding boundary conditions at both ends of TBB can be expressed as:

$$(N - \overline{N})\delta u = 0 \tag{14a}$$

$$\left[(M_\omega)' + M_t^P + \frac{1}{2}EI_{pp}\left(\theta_x'\right)^3 + EI_p'u'\theta_x' + EI_{p\chi}\chi'\theta_x' - \overline{M}_t - \overline{M}_\omega\right]\delta\theta_x = 0 \tag{14b}$$

$$\left[M_\Psi^\chi + \frac{1}{2}EI_{\chi\chi}(\chi_x')^3 + EI_\chi u'\chi' + EI_{p\chi}\chi'\theta_x' - \overline{M}_\chi\right]\delta\theta_x = 0 \tag{14c}$$

Where the geometric cross-sectional properties related to torsion and distortion I_{pp} and $I_{\chi\chi}$ are respectively expressed as:

$$I_{pp} = \int_\Omega \left(y^2 + z^2\right)^2 d\Omega \tag{15a}$$

$$I_{\chi\chi} = \int_\Omega \left(\eta_s^{i2} + \phi_s^{\chi i2}\right)^2 d\Omega \tag{15b}$$

In Equation (14), $\overline{N}$,$\overline{M}_t$,$\overline{M}_\omega$,$\overline{M}_\chi$ are variations of the conserved axial force, torsional moment, warping moment and distortion moment at the end of TBB over time, respectively. The expressions of the external load relative to the first Piola-Kirchhoff stress component can be easily derived from the Equation (13d). Significantly, the distribution of secondary shear stress was ignored when deriving the TBB governing

equation [25]. Regarding the initial boundary value problem, the relevant governing partial differential equation of TBB can be obtained through Equation (10) as:

$$\rho A\ddot{u} - EAu'' - EI_p\theta_x^{'}\theta_x^{''} - EI_\chi\chi^{'}\chi^{''} - EI_{px}\theta_x^{'}\chi^{''} - EI_{px}\theta_x^{''}\chi^{'} = n(x,t) \tag{16a}$$

$$\begin{aligned}&\rho I_p\ddot{\theta}_x + \rho C_s\ddot{\theta}_x^{''} - GI_t\theta_x^{''} - EC_s\theta_x^{IV} - \frac{3}{2}EI_{pp}(\theta_x^{'})^2\theta_x^{''} - EI_pu^{'}\theta_x^{''} - EI_pu^{''}\theta_x^{'} - EI_{p\chi}\theta_x^{''}\chi^{'} - EI_{p\chi}\theta_x^{'}\chi^{''}\\ &= m_t(x,t) + \frac{\partial m_\omega(x,t)}{\partial x}\end{aligned} \tag{16b}$$

$$\rho I_\chi\ddot{\chi} - GI_d\chi^{''} - \frac{3}{2}EI_{\chi\chi}(\chi^{'})^2\chi^{''} - EI_\chi u^{'}\chi^{''} - EI_\chi u^{''}\chi^{'} - EI_{p\chi}\theta_\chi^{'}\chi^{''} - EI_{p\chi}\theta_\chi^{''}\chi^{'} = m_\chi(x,t) \tag{16c}$$

Equation (16) are the coupled equilibrium equations of axial displacement, torsion and distortion, where the nonlinear term is retained as the third-order (such as $\theta_\chi^{'}\chi^{''}$, $\theta_\chi^{''}\chi^{'}$, $u^{'}\chi^{''}$…).

Subjected to the initial conditions ($x \in (0, l)$):

$$u(x,0) = \bar{u}_0(x) \tag{17a}$$

$$\dot{u}(x,0) = \dot{\bar{u}}_0(x) \tag{17b}$$

$$\theta_x(x,0) = \bar{\theta}_{x0}(x) \tag{17c}$$

$$\dot{\theta}_x(x,0) = \dot{\bar{\theta}}_{x0}(x) \tag{17d}$$

$$\chi(x,0) = \bar{\chi}_0(x) \tag{17e}$$

$$\dot{\chi}(x,0) = \dot{\bar{\chi}}_0(x) \tag{17f}$$

And the boundary conditions at both ends of TBB $x = 0, l$:

$$\alpha_1 N + \alpha_2 u = \alpha_3 \tag{18a}$$

$$\beta_1 M_t + \beta_2\theta_x + \bar{\beta}_1 M_\omega + \bar{\beta}_2\theta_x^{'} = \beta_3 + \bar{\beta}_3 \tag{18b}$$

$$\varphi_1 M_\Psi + \varphi_2\chi = \varphi_3 \tag{18c}$$

In which, N, M_t, M_w and M_ψ are axial force, torsional moment, warping and distortion moments at both ends of TBB, respectively, given as:

$$N = EAu_0^{'} + \frac{1}{2}EI_p\theta_x^{'2} + \frac{1}{2}EI_\chi\chi^{'2} + EI_{px}\theta_x^{'}\chi^{'} \tag{19a}$$

$$M_t = GI_t\theta_x^{'} - EC_s\theta_x^{'''} + EI_pu^{'}\theta_x^{'} + \frac{1}{2}EI_{pp}(\theta^{'})^3 + EI_{p\chi}\theta_x^{'}\chi^{''} \tag{19b}$$

$$M_\omega = -EC_s\cdot\theta^{''} \tag{19c}$$

$$M_\Psi = GI_d\chi^{'} + EI_\chi u^{'}\chi^{'} + \frac{1}{2}EI_{\chi\chi}(\chi^{'})^3 + EI_{p\chi}\theta_\chi^{''}\chi^{'} \tag{19d}$$

Where, α_j, β_j, $\overline{\beta}_j$,φ_j (j = 1, 2, 3) are time-varying functions corresponding to the TBB boundary, respectively. The boundary conditions in this paper are the very general boundary conditions of the discussed problem, including elastic supports. Obviously, after appropriately specifying the function (for simply supported edges $\beta_2 = \bar{\beta}_1 = 1$, $\beta_1 = \beta_3 = \overline{\beta}_2 = \overline{\beta}_3 = 0$), all kinds of regular torsional boundary conditions can be derived from Equation (15). At this point, the warping is completely limited at the clamped edge (that is $u = 0$). In this way, the term $\theta^{'} \cdot \phi_s^P$ in Equation (1a) must disappear. That is to say, if the clamping edge is a warping boundary condition, then this factor is mathematically satisfied. If $\theta' = 0$, then this is the exact expression. It can be known from Equation (19) that the boundary condition terms of Equation (18) is nonlinear, and there is no special difficulty in adding damping to Equation (13).

When calculating the unknown displacement components, the the initial boundary value problem shown in Equations (16)–(18) can be solved. The constants C_s and I_t defined by Equation (11) indicate that after solving the boundary value problem in Equation (4), if the primary warping function ϕ_s^P is found at any internal point in the domain Ω, the above constants can be evaluated. As long as $u(x,t)$, $\theta_x(x,t)$, $\chi(x,t)$ are analyzed, the stress components and the displacement field are obtained by Equations (3) and (1), respectively.

Such initial boundary value problems have strong coupling and nonlinearity. The differential equation system can be significantly reduced by ignoring the axial inertia term $\rho A \cdot \ddot{u}$ of Equation (13a), which is a frequently used assumption in the dynamic girder formula. Omitting the term, the partial differential equations of the unknown displacement component (torsion angle $\theta_x(x,t)$ and distortion angle $\chi(x,t)$) are obtained. When the axial load distributed along the TBB direction disappears, the equation is further simplified. In the following chapters, the simple support conditions and the axial constant load along the TBB are described in detail. This paper incorporates the problem of nonlinear and non-uniform torsional vibration into the numerical analysis section for the first time to study its neglected influence.

2.5. Simplified initial-boundary value problems under axial boundary conditions

The axial boundary condition (16a) at the axial immovable end can be expressed as:

$$u(x,0) = 0 \tag{20a}$$

$$u(l,0) = 0 \tag{20b}$$

It is given according to the simplified Equation (16a) mentioned earlier.

$$u_0^{''} = -\frac{I_p}{A}\theta_x^{'}\theta_x^{''} - \frac{I_x}{A}\chi^{'}\chi^{''} - \frac{I_{px}}{A}\theta_x^{'}\chi^{''} - \frac{I_{px}}{A}\theta_x^{''}\chi^{'},\ \forall x \in (0,l) \tag{21}$$

Subsequently, by integrating and utilizing Equation (17), that can be written as:

$$u_0^{'} = -\frac{1}{2}\frac{I_\rho}{A}(\theta_x^{'})^2 - \frac{1}{2}\frac{I_\chi}{A}(\chi^{'})^2 - \frac{I_{\rho\chi}}{A}\theta_x^{'}\chi^{'} + \frac{\widetilde{N}}{EA},\ \forall x \in (0,l) \tag{22}$$

Where, $\widetilde{N}$ is the axial tensile load that varies with time due to geometrical nonlinearity, that expressed as:

$$\widetilde{N} = \frac{1}{2}\frac{EI_p}{l}\int_0^l (\theta_x')^2 dx + \frac{1}{2}\frac{EI_\chi}{l}\int_0^l (\chi')^2 dx + \frac{EI_{p\chi}}{l}\int_0^l (\theta_x'\chi')dx \tag{23}$$

Under the condition of a constant axial load in TBB, Equation (21) holds, and the axial boundary condition Equation (18a) is:

$$u_0(x,0) = 0 \tag{24a}$$

$$N(l,t) = \bar{N}(l,t) \tag{24b}$$

Therefore, Equation (22) is established through the setting of $\widetilde{N} = \bar{N}(l,t)$.

By substituting Equations (21) and (22) into Equations (16b) and (19b), the simplified initial boundary value problem can be expressed as:

$$\begin{aligned}
&\rho I_p \ddot{\theta}_x - \rho C_s \ddot{\theta}_x'' - \left(GI_t + \frac{I_p\widetilde{N}}{A}\right)\theta_x'' + \frac{EI_pI_\chi}{A}\theta_x'\chi'\chi'' \\
&-\frac{3}{2}E\left[I_{pp} - \frac{I_p^2}{A}\right](\theta_x')^2\theta_x'' + \frac{1}{2}\frac{EI_pI_\chi}{A}(\chi')^2\theta_x'' \\
&+2\frac{EI_pI_{p\chi}}{A}\theta_x'\theta_x''\chi' + \frac{EI_pI_{p\chi}}{A}(\theta_x')^2\chi'' + EC_s\theta_x^{IV} \\
&-EI_{p\chi}\theta_x''\chi' - EI_{p\chi}\theta_x'\chi'' = m_t(x,t) + \frac{\partial m_\omega(x,t)}{\partial x}
\end{aligned} \tag{25a}$$

$$\begin{aligned}
&\rho I_\chi \ddot{\chi} - \left(GI_d + \frac{I_\chi\widetilde{N}}{A}\right)\chi'' - \frac{3}{2}E\left[I_{\chi\chi} - \frac{I_\chi^2}{A}\right](\chi')^2\chi'' + \frac{1}{2}\frac{EI_\chi I_p}{A}(\theta_x')^2\chi'' + \frac{2EI_\chi I_{p\chi}}{A}\theta_x'\chi'\chi'' \\
&+\frac{EI_\chi I_p}{A}\theta_x'\theta_x''\chi' + \frac{EI_\chi I_{p\chi}}{A}\theta_x''(\chi')^2 - EI_{p\chi}\theta_x'\chi'' - EI_{p\chi}\theta_x''\chi' = m_\chi(x,t)
\end{aligned} \tag{25b}$$

Analyzing the equilibrium of torsion and distortion, the vibration equilibrium Equation (25) retain the fourth-order nonlinear terms of torsion and distortion, such as $\theta_x'\chi'\chi''$, $(\theta_x')^2\chi''$, $(\chi')^2\theta_x''$… Considering these nonlinear terms is conducive to accurately analyzing torsion and distortion warping deformations.

Comparing Equations (25) and (19) with the corresponding set presented by Rozmarynowski and Szymczak [1] and Sapountzakis and Mokos [7], the corresponding improvements have been made

- In Rozmarynowski and Szymczak's research [1], the elastic support situation does not exist in the torsional and warpage boundary conditions.
- In Sapountzakis and Mokos's research [7], the nonlinear terms related to finite torsional rotation do not exist in the distorted boundary conditions.
- Ignoring the axial inertia term does not have an impact on the torsional moment. The impact of these terms will follow numerical research.

3. Integral numerical solution

3.1. The axial displacement u, the twist angle θ and distortion angle χ

On the basis of the aforementioned analysis, the displacement components u_m, θ and χ respectively have continuous second-order partial derivatives on t and continuous second-order and fourth-order partial derivatives on x, and satisfy the nonlinear initial boundary value problem along the TBB in the coupled control Equation (16), the nonlinear non-uniform torsional vibration problem of the TBB is alleviated.

Use hyperbolic differential equations to solve the simulation equation of Equations (16)–(18). In the light of this method, let $u(x,t)$, $\theta_x(x,t)$ and $\chi(x,t)$ be the solutions of the above problems. Let $u_1(x,t) = u(x,t)$, $u_2(x,t) = \theta_x(x,t)$, $u_3(x,t) = \chi(x,t)$ take the derivative of x twice and four times, respectively, then:

$$\frac{\partial^2 u_1}{\partial x^2} = q_1(x,t) \tag{26a}$$

$$\frac{\partial^4 u_2}{\partial x^4} = q_2(x,t) \tag{26b}$$

$$\frac{\partial^2 u_3}{\partial x^2} = q_3(x,t) \tag{26c}$$

Equation (24) are quasi-static, which means that the time variable is taken as the parameter. The results show as long as the virtual distributed load $q_j(x,t)$ (j = 1, 2, 3) is established first, the solutions of Equations (16)–(18) can be obtained by solving Equation (26) under the same boundary condition (18). These distributions can be solved by the boundary element method, as shown below.

The solutions of Equation (26) expressed in integral form are:

$$u_1(x,t) = \int_0^l q_1 u_1^* d\xi - \left[u_1^* \frac{\partial u_1}{\partial x} - \frac{du_1^*}{\partial x} u_1 \right]_{x=0}^{x=l} \tag{27a}$$

$$u_2(x,t) = \int_0^l q_2 u_2^* d\xi - \left[u_2^* \frac{\partial^3 u_2}{\partial x^3} - \frac{du_2^*}{dx} \frac{\partial^2 u_2}{\partial x^2} + \frac{d^2 u_2^*}{dx^2} \frac{\partial u_2}{\partial x} - \frac{d^3 u_2^*}{dx^3} u_2 \right]_0^l \tag{27b}$$

$$u_3(x,t) = \int_0^l q_3 u_3^* d\xi - \left[u_3^* \frac{\partial u_3}{\partial x} - \frac{du_3^*}{\partial x} u_3 \right]_{x=0}^{x=l} \tag{27c}$$

In which, u_1^*, u_2^*, u_3^* are the basic solutions expressed as:

$$u_1^* = u_3^* = \frac{1}{2}|r| \tag{28a}$$

$$u_2^* = \frac{1}{12} l^3 \left(2 + \left| \frac{r}{l} \right|^3 - 3 \left| \frac{r}{l} \right|^2 \right) \tag{28b}$$

When $r = x - \xi$ of TBB is at the points of x, ξ, the particular singular solutions of the equations are expressed as:

$$\frac{\partial^2 u_1^*}{\partial x^2} = \frac{\partial^2 u_3^*}{\partial x^2} = \delta(x - \xi) \tag{29a}$$

$$\frac{\partial^4 u_2^*}{\partial x^4} = \delta(x-\xi) \tag{29b}$$

By using Equation (26), the integral representations of Equation (25) can be obtained.

$$u_1 = \int_0^1 q_1 \left(\Lambda_2(r) + \frac{1}{2}l\right) d\xi - \left[\left(\Lambda_2(r) + \frac{1}{2}l\right)\frac{\partial u_1}{\partial x} + \Lambda_1(r)u_1\right]_0^l \tag{30a}$$

$$u_2 = \int_0^1 q_2 \Lambda_4(r) d\xi - \left[\Lambda_4(r)\frac{\partial^3 u_2}{\partial x^3} + \Lambda_3(r)\frac{\partial^2 u_2}{\partial x^2} + \Lambda_2(r)\frac{\partial u_2}{\partial x} + \Lambda_1(r)u_2\right]_0^l \tag{30b}$$

$$u_3 = \int_0^1 q_3 \left(\Lambda_2(r) + \frac{1}{2}l\right) d\xi - \left[\left(\Lambda_2(r) + \frac{1}{2}l\right)\frac{\partial u_3}{\partial x} + \Lambda_1(r)u_3\right]_0^l \tag{30c}$$

Where, $\Lambda_j(r)$ (j = (1, 2, 3, 4)) are the kernels, those are given in **Appendix A**. In Equation (30), for a line integral it is $r = x - \xi$, (x, ξ points of TBB), and for the rest of the item, it is $r = x - \xi$, (x inside the beam, ξ at the ends of TBB 0, l).

Taking the differentiate of Equation (30) with respect to x gives an integral representations of the derivatives of u_j as:

$$\frac{\partial u_1(x,t)}{\partial x} = \int_0^1 q_1 \Lambda_1(r) d\xi - \left[\Lambda_1(r)\frac{\partial u_1}{\partial x}\right]_{x=0}^{x=l} \tag{31a}$$

$$\frac{\partial^2 u_1}{\partial x^2} = q_1(x,t) \tag{31b}$$

$$\frac{\partial u_2(x,t)}{\partial x} = \int_0^1 q_2 \Lambda_3(r) d\xi - \left[\Lambda_3(r)\frac{\partial^3 u_2}{\partial x^3} + \Lambda_2(r)\frac{\partial^2 u_2}{\partial x^2} + \Lambda_1(r)\frac{\partial u_2}{\partial x}\right]_0^l \tag{31c}$$

$$\frac{\partial^2 u_2(x,t)}{\partial x^2} = \int_0^1 q_2 \Lambda_2(r) d\xi - \left[\Lambda_2(r)\frac{\partial^3 u_2}{\partial x^3} + \Lambda_1(r)\frac{\partial^2 u_2}{\partial x^2}\right]_0^l \tag{31d}$$

$$\frac{\partial^3 u_2(x,t)}{\partial x^3} = \int_0^1 q_2 \Lambda_1(r) d\xi - \left[\Lambda_1(r)\frac{\partial^3 u_2}{\partial x^3}\right]_0^l \tag{31e}$$

$$\frac{\partial^4 u_2}{\partial x^4} = q_2(x,t) \tag{31f}$$

$$\frac{\partial u_3(x,t)}{\partial x} = \int_0^1 q_3 \Lambda_1(r) d\xi - \left[\Lambda_1(r)\frac{\partial u_3}{\partial x}\right]_{x=0}^{x=l} \tag{31g}$$

$$\frac{\partial^2 u_3}{\partial x^2} = q_3(x,t) \tag{31h}$$

Applied to the integral representations (30) and (31) of TBB's ends (0,l), combined with the boundary conditions (18), q_j is used to represent the unknown boundary quantities $u_j(\xi,t)$, $u_{jx}(\xi,t)$, $u_{2,xx}(\xi,t)$ and $u_{2,xxx}(\xi,t)$ (ξ = 0). This is numerically

implemented as follows.

As shown in **Figure 2**, the interval (0,*l*) can be divided into *L* elements. It is assumed that q_j(x,t) changes in light of certain rules, such as constant, linear, parabolic,etc.. It can be known from the research conducted by Sapountzakis and Dikaros [9] that selection of the constant element hypothesis makes the numerical implementation very simple and can obtain better results. Therefore, the constant element is also selected in this paper.

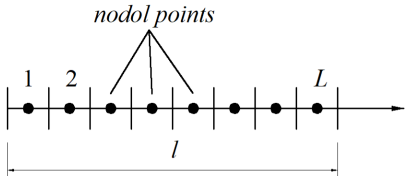

Figure 2. Interval discretization and node distribution of the TBB.

Using the above method, the following 15 nonlinear algebraic equations can be obtained:

$$\begin{Bmatrix} \mathbf{0} \\ \boldsymbol{\alpha}_3 \\ \mathbf{0} \\ \boldsymbol{\beta}_3+\bar{\boldsymbol{\beta}}_3 \\ \mathbf{0} \\ \boldsymbol{\varphi}_3 \end{Bmatrix} = \begin{bmatrix} \mathbf{F}_1 & \mathbf{E}_{12} & \mathbf{E}_{12} & & & & & & & & & & \\ & \mathbf{D}_{22} & \mathbf{D}_{23} & & & & & & & & & & \\ & & & \mathbf{F}_3 & \mathbf{E}_{35} & \mathbf{E}_{36} & \mathbf{E}_{37} & \mathbf{E}_{38} & & & & & \\ & & & & \mathbf{D}_{45} & \mathbf{D}_{46} & \mathbf{D}_{47} & \mathbf{D}_{48} & & & & & \\ & & & & & & & & \mathbf{F}_5 & \mathbf{E}_{59} & \mathbf{E}_{510} & \mathbf{E}_{511} \\ & & & & & & & & & \mathbf{D}_{69} & \mathbf{D}_{610} & \mathbf{D}_{611} \end{bmatrix} \begin{Bmatrix} \boldsymbol{q}_1 \\ \hat{\boldsymbol{u}}_1 \\ \hat{\boldsymbol{u}}_{1,x} \\ \boldsymbol{q}_2 \\ \hat{\boldsymbol{u}}_2 \\ \hat{\boldsymbol{u}}_{2,x} \\ \hat{\boldsymbol{u}}_{2,xx} \\ \hat{\boldsymbol{u}}_{2,xxx} \\ \boldsymbol{q}_3 \\ \hat{\boldsymbol{u}}_3 \\ \hat{\boldsymbol{u}}_{3,x} \end{Bmatrix} + \begin{bmatrix} \mathbf{D}_{21}^{nl} & \mathbf{D}_{22}^{nl} & \mathbf{D}_{23}^{nl} & & & & & & & & \\ & & & \mathbf{D}_{43}^{nl} & \mathbf{D}_{44}^{nl} & \mathbf{D}_{45}^{nl} & & & & & \\ & & & \mathbf{D}_{63}^{nl} & & & & & \mathbf{D}_{66}^{nl} & \mathbf{D}_{67}^{nl} & \end{bmatrix} \begin{Bmatrix} \hat{\boldsymbol{u}}_2^2 \\ \hat{\boldsymbol{u}}_3^2 \\ \hat{\boldsymbol{u}}_2\hat{\boldsymbol{u}}_3 \\ \hat{\boldsymbol{u}}_2^3 \\ \hat{\boldsymbol{u}}_1\hat{\boldsymbol{u}}_2 \\ \hat{\boldsymbol{u}}_1\hat{\boldsymbol{u}}_3 \\ \hat{\boldsymbol{u}}_3^3 \end{Bmatrix} \tag{32}$$

Where, $\mathbf{D}_{m\times n}$(m,n = 1,2,3…) and $\mathbf{D}^{nl}_{m\times n}$ are 2 × 2 known matrices , usually containing the values of the functions $\alpha_j, \beta_j, \bar{\beta}_j, \varphi_j$($j$ = 1,2) of Equation (18a), that is, the time-dependent matrices. $\alpha_3, \beta_3, \bar{\beta}_3, \varphi_3$ are 2 × 1 known column matrices, usually related to time, including the boundary values of the functions; $\mathbf{E}_{m\times n}$ is rectangular 2 × 2 known coefficient matrix generated by the values of the kernels $\Lambda_j(r)$, and $\mathbf{F}_m$ are 2 × L rectangular known matrices generating by the integral of the kernels on the axis of TBB. In addition:

$$\hat{\mathbf{u}}_i = \{u_i(0,t) \quad u_i(l,t)\}^T \quad (i=1,2,3) \tag{33a}$$

$$\hat{\mathbf{u}}_{i,x} = \left\{ \frac{\partial u_i(0,t)}{\partial x} \quad \frac{\partial u_i(l,t)}{\partial x} \right\}^T \quad (i=1,2,3) \tag{33b}$$

$$\hat{\mathbf{u}}_{2,xx} = \left\{ \frac{\partial^2 u_2(0,t)}{\partial x^2} \quad \frac{\partial^2 u_2(l,t)}{\partial x^2} \right\}^T \tag{33c}$$

$$\widehat{\mathbf{u}}_{2,xxx} = \left\{ \frac{\partial^3 u_2(0,t)}{\partial x^3} \quad \frac{\partial^3 u_2(l,t)}{\partial x^3} \right\}^T \tag{33d}$$

$$\widehat{\mathbf{u}}_2^2 = \left\{ \left[\frac{\partial u_2(0,t)}{\partial x}\right]^2 \quad \left[\frac{\partial u_2(l,t)}{\partial x}\right]^2 \right\}^T \tag{33e}$$

$$\widehat{\mathbf{u}}_2^3 = \left\{ \left[\frac{\partial u_2(0,t)}{\partial x}\right]^3 \quad \left[\frac{\partial u_2(l,t)}{\partial x}\right]^3 \right\}^T \tag{33f}$$

$$\widehat{\mathbf{u}}_1\widehat{\mathbf{u}}_2 = \left\{ \frac{\partial u_1(0,t)}{\partial x} \cdot \frac{\partial u_2(0,t)}{\partial x} \; \frac{\partial u_2(0,t)}{\partial x} \cdot \frac{\partial u_1(0,t)}{\partial x} \right\}^T \tag{33g}$$

$$\widehat{\mathbf{u}}_3^3 = \left\{ \left[\frac{\partial u_3(0,t)}{\partial x}\right]^3 \quad \left[\frac{\partial u_3(l,t)}{\partial x}\right]^3 \right\}^T \tag{33h}$$

$$\widehat{\mathbf{u}}_1\widehat{\mathbf{u}}_3 = \left\{ \frac{\partial u_1(0,t)}{\partial x} \cdot \frac{\partial u_3(0,t)}{\partial x} \; \frac{\partial u_3(0,t)}{\partial x} \cdot \frac{\partial u_1(0,t)}{\partial x} \right\}^T \tag{33i}$$

$$\widehat{\mathbf{u}}_2\widehat{\mathbf{u}}_3 = \left\{ \frac{\partial u_2(0,t)}{\partial x} \cdot \frac{\partial u_3(0,t)}{\partial x} \; \frac{\partial u_3(0,t)}{\partial x} \cdot \frac{\partial u_2(0,t)}{\partial x} \right\}^T \tag{33j}$$

The above formulas are vectors containing two unknown time-varying boundary values containing their respective boundary quantities and $q_i = \{q_1^i \; q_2^i \ldots q_l^i\}^{\mathrm{T}} (i = 1,2,3)$ are vectors containing the L unknown time-varying nodal values of the virtual loads.

By using Equation (16) to L match points, $2L$ semi-discrete nonlinear equations of motion are expressed by Equations (32) and (33) as:

$$\mathbf{M} \begin{bmatrix} \ddot{\mathbf{d}}_1 \\ \ddot{\mathbf{d}}_2 \\ \ddot{\mathbf{d}}_3 \end{bmatrix} + \mathbf{K} \begin{Bmatrix} \mathbf{d}_1 \\ \mathbf{d}_2 \\ \mathbf{d}_3 \end{Bmatrix} + \mathbf{k}^{nl}(\mathbf{H}_1^i, \mathbf{H}_2^j, \mathbf{H}_3^i, \mathbf{d}_1, \mathbf{d}_2, \mathbf{d}_3) = \mathbf{f} \tag{34}$$

Where $\mathbf{d}_1^T = \{\mathbf{q}_1 \; \widehat{\mathbf{u}}_1 \; \widehat{\mathbf{u}}_{1,\mathbf{x}}\}$, $\mathbf{d}_2^T = \{\mathbf{q}_3 \; \widehat{\mathbf{u}}_2 \; \widehat{\mathbf{u}}_{2,x} \; \widehat{\mathbf{u}}_{2,xx} \; \widehat{\mathbf{u}}_{2,xxx}\}$, $\mathbf{d}_3^T = \{\mathbf{q}_3 \; \widehat{\mathbf{u}}_3 \; \widehat{\mathbf{u}}_{3,x}\}$ are generalized unknown vectors and $\mathbf{H}_1^i$, $\mathbf{H}_3^i$ are $L \times (L + 4)$ known matrices and is $L \times (L + 8)$ known matrices, respectively. $\mathbf{M}$ is generalized mass matrix. $\mathbf{K}$ is stiffness matrix. $\mathbf{k}^{nl}$ is a nonlinear generalized stiffness vector and $\mathbf{f}$ is force vector. Those have been expressed in **Appendix B**.

Therefore, when $t = 0$, Equation (17) yields the following $2L$ linear equations for $\mathbf{d}_1$, $\mathbf{d}_2$, $\mathbf{d}_3$:

$$\mathbf{H}_1^0 \mathbf{d}_1 = \overline{\mathbf{u}}_0 \tag{35a}$$

$$\mathbf{H}_2^0 \mathbf{d}_2 = \overline{\boldsymbol{\theta}}_0 \tag{35b}$$

$$\mathbf{H}_3^0 \mathbf{d}_3 = \overline{\boldsymbol{\chi}}_0 \tag{35c}$$

The aforementioned equations and Equation (32) for $t = 0$ form a set of $2L + 12$ nonlinear algebraic equations. The initial conditions $\mathbf{d}_1(0)$, $\mathbf{d}_2(0)$, $\mathbf{d}_3(0)$ are established to solve these equations. Similarly, when combined with Equation (17), for $t = 0$, the

following $2L$ linear equations about $\dot{\mathbf{d}}_1$,$\dot{\mathbf{d}}_2$,$\dot{\mathbf{d}}_3$ are obtained:

$$\mathbf{H}_1^0\dot{\mathbf{d}}_1(0) = \dot{\bar{\mathbf{u}}}_0(0) \tag{36a}$$

$$\mathbf{H}_2^0\dot{\mathbf{d}}_2(0) = \dot{\bar{\boldsymbol{\theta}}}_0(0) \tag{36b}$$

$$\mathbf{H}_3^0\dot{\mathbf{d}}_3(0) = \dot{\bar{\boldsymbol{\chi}}}_0(0) \tag{36c}$$

The aforementioned equations and the 12 equations that Equation (32) takes with respect to time and is written at $t = 0$ are composed of a set of 2L + 12 linear algebraic equations from which the initial conditions $\dot{\mathbf{d}}_1(0)$,$\dot{\mathbf{d}}_2(0)$,$\dot{\mathbf{d}}_3(0)$ are set up. Note that, general speaking, $\mathbf{d}_1(0)$, $\mathbf{d}_2(0)$, $\mathbf{d}_3(0)$ must be used to analyze the system of equations.

The above initial conditions and Equations (32) and (34) constitute the initial value problem of the differential algebraic equation (DAE), which could be calculated by effective solver. When solving, a new variable can be introduced to reduce the order of the system, enabling the Petzold-Gear method to differentiate Equation (32) with respect to time. Thus, an equivalent system with the system index = 1 [9] can be obtained.

3.1.1. Reduce the initial vibration boundary value

The simplified initial boundary value problem described in Equations (13)–(15) can be similarly analyzed and solved in a similar way according to the above steps. In addition, for free vibrations, the existence of a motion reversal point can be assumed, so it can be defined as follows:

$$\dot{\theta}_{\max} = 0 \tag{37a}$$

$$\ddot{\theta}_{\max} = -\omega^2 \cdot \theta_{\max} \tag{37b}$$

$$\dot{\chi}_{\max} = 0 \tag{37c}$$

$$\ddot{\chi}_{\max} = -\omega^2 \cdot \chi_{\max} \tag{37d}$$

In which, the subscript max represents the points where the motion inversion occurs and ω^2 represents the sample size of the eigenvalue characterizing the nonlinear strength. It can be seen that this is different from the natural frequency of TBB, because Equation (25) obviously does not allow variables to be factorized. Similarly, a single harmonic is brought into Equation (25) and considering that m_t, m_ω and m_χ along with $\beta_3, \bar{\beta}_3, \varphi_3$ disappear separately, the nonlinear generalized eigenvalue problem could be expressed as:

$$[\mathbf{K}_\theta^L + \mathbf{K}_\theta^{NL} - \omega^2\mathbf{M}_\theta]\mathbf{d}_2 = \mathbf{0} \tag{38a}$$

$$[\mathbf{K}_\chi^L + \mathbf{K}_\chi^{NL} - \omega^2\mathbf{M}_\chi]\mathbf{d}_3 = \mathbf{0} \tag{38b}$$

Where $\mathrm{K}_\theta^{\mathrm{NL}}$,$\mathrm{K}_\chi^{\mathrm{NL}}$ are nonlinear stiffness matrices and $\mathrm{K}_\theta^{\mathrm{L}}$,$\mathrm{K}_\chi^{\mathrm{L}}$,$\mathrm{M}_\theta$,$\mathrm{M}_\chi$ are stiffness and mass matrices, in **Appendix B**.

Although the eigenvalue problem of Equation (38) shows the nonlinear behavior

of TBB, the time-domain solution is not provided. This is because the modal shapes and eigenvalues are related to the amplitudes of the initial conditions. It should be noted here that the required frequency is different from the actual natural frequency. For the axially immovable ends, $\widetilde{N}$ adopts the discretization and constant assumption of the above-mentioned beams in each iteration, and the numerical integration of Equation (23) can be used for calculation.

3.1.2. Reduce the initial vibration boundary value

It can be known from Equation (11) that for the calculation of the above constants, it is assumed that at any internal point in the Ω region of the TBB cross-section. the primary warping function ϕ_s^{Pi} is known . Once ϕ_s^{Pi} is established, according to the corresponding relationship given in Sapountzakis and Dikaros's study [9], the field integral is transformed along the boundary into a line integral, thereby calculating the C_s and I_t constants. In addition, when calculating the stress component, the BEM [7] is used to calculate the values of ϕ_s^{Pi} at any internal point about the shear center *S* and its derivatives about *n* and *s*, as shown in Sapountzakis et al. [6]. At last, the nonlinear torsional vibrations problem is analyzed by using the BEM, and the domain integrals of Equations (11) and (16) must be transformed into boundary integrals by using the partial, the Green identity and the Gauss theorem, and the expressed as:

$$I_t = \frac{b^3 t_1 + h^3 t_2}{12} \tag{39a}$$

$$C_s = \frac{h^2 b^3 t_1 + b^2 h^3 t_2}{3 * 2^4} \tag{39b}$$

4. Numerical examples

On the basis of the analytical and numerical procedures introduced in the aforementioned sections, representative examples are analyzed to demonstrate the effectiveness of considering nonlinearities and distortion, and where possible to verify and apply the range. In addition, assuming that the TBB material is within the elastic range, except for some extreme deformations, it is considered that the strain is very small regardless of the magnitude of angle of twist θ_x.

In all calculation examples, the geometric dimensions of TBB are shown in **Figure 3**. The material properties are $E = 2.1 \times 10^8$ kNm^{-2}, $G = 8.1 \times 10^7$ kNm^{-2}, $\rho = 8.002$ kNs^{2}m^{-4}. The numerical results were obtained using 21 nodal points (longitudinal discretization) and 400 boundary elements (cross-section discretization).

4.1. Example 1

In this example, the free vibrations of TBB under different boundary conditions were analyzed and compared. In more detail, to obtain the dynamic characteristics at the motion reversal points, the generalized eigenvalue problem of Equation (38) is solved (i.e., the initial boundary value problem was simplified). Firstly, the component has a simply supported torsional boundary condition. Considering all the nonlinear terms of Equation (25), **Table 1** presents the linear and five nonlinear cases with different initial torsional midpoint angles $\bar{\theta}_{x0}(l/2)$ amplitudes, the fundamental natural frequency ω

of the TBB axial stationary end and the induced axial load $\widetilde{N}$ of simply supported torsional boundary condition. **Table 2** presents the basic natural frequencies of TBB with simply supported torsional boundary conditions. The beam has different initial torsional amplitude midpoint angles $\bar{\theta}_{x0}(l/2)$ and different load values under linear and five nonlinear cases (one end is a constant time-axial load $\bar{N}(l,t)$, the other end is tensile, disappearance and compression), and the last load corresponds to the buckling state after torsion, which proves the validity of the proposed formulation.

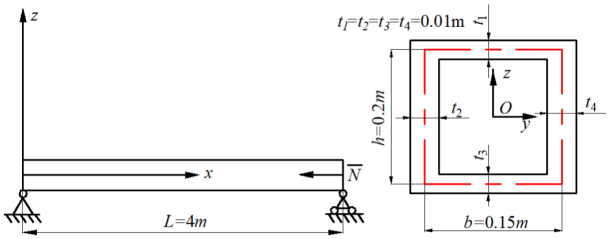

Figure 3. Thin-walled box beam: geometry and loading.

Table 1. Basic natural frequency $\omega(s^{-1})$ and induced axial load $\widetilde{N}$(kN) of TBB with simply torsional boundary conditions and axially immovable ends.

$\theta_{x0}(l/2)(rad)$		Present study		Sapountzakis and Dikaros [9]	Rozmarynowski and Szymczak [1]
		Considering nonlinear terms	*Ignoring nonlinear terms*		
0.1	ω	118.93	118.09	117.43	116.57
	$\widetilde{N}$	21.45	21.32	23.16	23.16
0.2	ω	126.41	123.22	120.66	117.32
	$\widetilde{N}$	90.80	90.93	92.63	93.18
0.5	ω	169.80	154.46	155.38	146.86
	$\widetilde{N}$	576.22	577.38	578.95	579.00
1.0	ω	273.37	234.16	237.63	222.34
	$\widetilde{N}$	2312.42	2313.01	2315.81	2386.90
1.5	ω	388.88	326.27	333.81	293.22
	$\widetilde{N}$	4851.69	4916.01	5126.53	5279.12

Table 2. Fundamental natural frequency of the thin-walled box beam with simple torsional boundary conditions and constant axial load.

	$\widetilde{N}$(kN)									
	−2000		−1000		0		1000		2000	
$\theta_{x0}(l/2)(rad)$	Sapountzakis and Dikaros [9]	Present study	Sapountzakis and Dikaros [9]	Present study	Sapountzakis and Dikaros [9]	Present study	Sapountzakis and Dikaros [9]	Present study	Sapountzakis and Dikaros [9]	Present study
0.1	252.39	257.33	232.31	242.15	201.38	207.59	161.07	169.90	130.96	136.97
0.2	260.06	267.12	237.92	243.10	206.33	208.49	168.35	172.28	140.46	142.76
0.5	284.83	293.18	254.96	261.85	214.77	221.38	194.87	196.12	154.22	169.34
1.0	319.07	324.40	293.35	300.35	257.72	262.01	213.35	217.83	185.23	190.46
1.5	356.55	368.53	327.00	335.65	309.53	314.47	263.22	274.09	215.62	222.62

In **Table 1**, the results obtained from the Rozmarynowski and Szymczak [1] that ignores the geometric cross-sectional constant and the the proposed method of Sapountzakis and Dikaros [9] that ignores the distortion confirm the proposed formula (the inconsistency of the values is due to the inaccuracy of the Vlasov's thin-walled beam theory adopted by Rozmarynowski and Szymczak [1]). In addition, the influence

of the nonlinear terms related to the geometric cross-sectional constant is noticed, especially in the case of large amplitude vibration. It is important to note that in **Table 2**, in the post-buckling case, the initial midpoint angle of the torsion amplitude cannot be arbitrary because it must be greater than the midpoint angle corresponding to the static (post-buckling) equilibrium state.

Note that in **Tables 1** and **2** above, it is easy to verify that the geometrical nonlinearity changes the modal shape of vibration, stiffening the structure and resulting in higher natural frequencies, which is the main aspect of nonlinear torsional free vibration analysis. Obviously, these effects are more pronounced with the increase of the initial midpoint angle of twist amplitude.

Figures 4–7 show the time histories of torsional amplitude, axial displacement, torsion moment and distortion moment of 5 initial torsional midpoint angles of different initial torsional amplitude ($\bar{\theta}_{x0}(l/2)$ = 0.1 rad, 0.2 rad, 0.5 rad, 1.0 rad, 1.5 rad) under different initial torsional rotation, and analyzes the two cases. In other words, the method proposed in this paper is used for linear analysis, ignoring the nonlinear term of Equation (16b,c) and Equations (25a,b), (17b,c), and (18b,c) are nonlinear simplified to the initial boundary value problem. For these cases, assume that the axial load N is equal to 0. From these figures, it can be seen the influence of nonlinear terms and distortion angles on motion components and stress components. In addition, from **Figure 4**, the natural frequency of the angle of the torsion angle $\theta_x(l/2, t)$ is calculated as the values ω of this study in **Table 1**. Therefore, as mentioned earlier, the solution to the eigenvalue problem of the equation can obtain a frequency-like value Equation (38a,b), but it cannot be confused with the actual natural frequency of TBB. Importantly, the apparent change in the torsional moment time-history pattern and the small change in torsional angle amplitude (It is not clearly shown in **Figure 4**) are due to the non-coincidence of the basic nonlinear mode shape and the linear mode shape.. In addition, it can be easily verified from **Figure 5** that the linear result of the axial displacement response amplitude is much larger than nonlinear result.

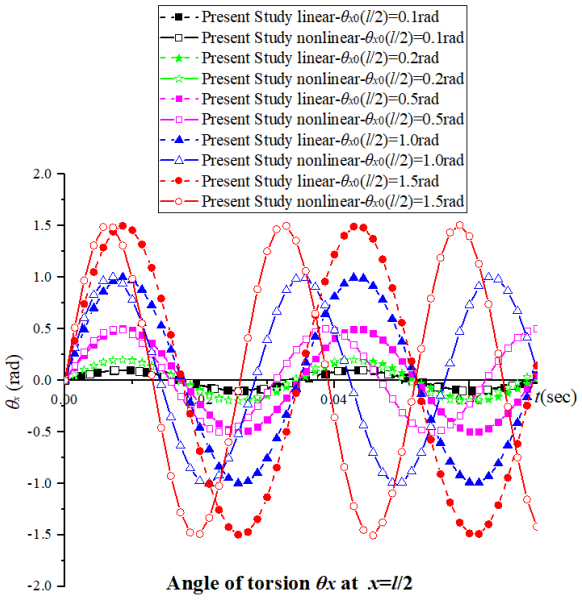

Figure 4. Time histories of the angle of torsion at the midpoint for the cases of different initial torsional rotation.

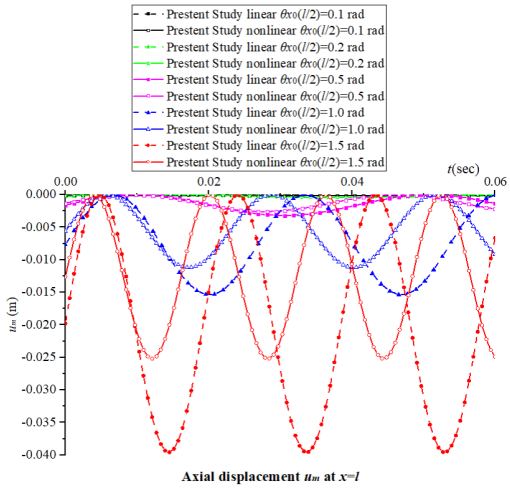

Figure 5. Time histories of the axial displacement for the cases of different initial torsional rotation.

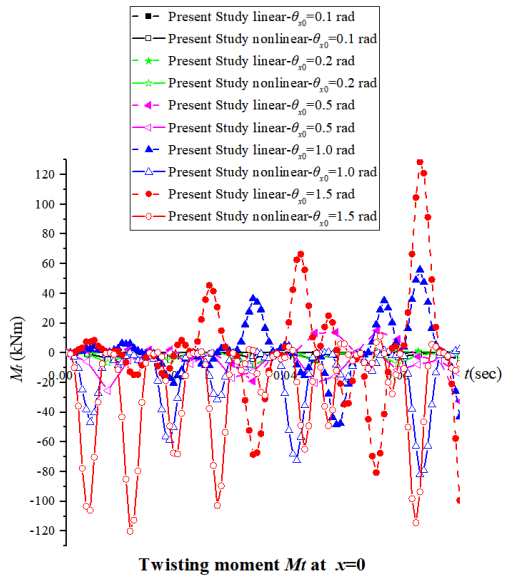

Figure 6. Time histories of the torsion moment for the cases of different initial torsional rotation.

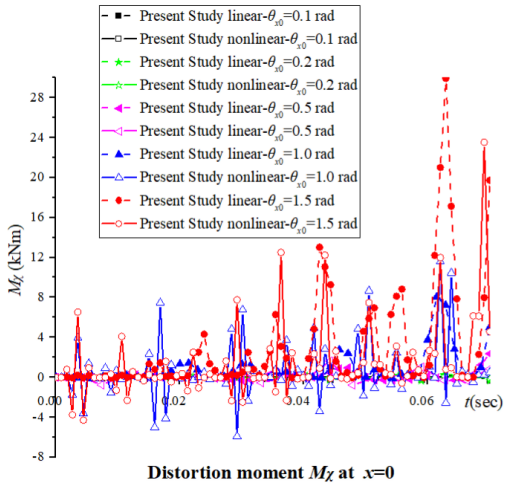

Figure 7. Time histories of the distortion moment for the cases of different initial torsional rotation.

In **Figures 6** and **7**, the time history of the torque and distortion moments shows that the linear and nonlinear values are so different. The main effective terms are in Equation (19b,d): $\frac{1}{2}EI_{pp}(\theta')^3$, $EI_{p_x}\theta'_x\chi''$, $\frac{1}{2}EI_{\chi\chi}(\chi')^3$, $EI_{p_x}\theta''_x\chi'$. It is obviously that the nonlinear terms $\frac{1}{2}EI_{pp}(\theta')^3$, $EI_{p_x}\theta'_x\chi''$ have an effect on the torsion moments, especially when the torsion angle $\theta_x(l/2, t)$ is greater than 0.5. Compared with the torque, the value of distortion moment is much smaller. This means that although the effect of distortion deformation on vibration of TBB is less than that of torsion deformation, the effect on TBB can not be ignored.

4.2. Example 2

The second example studies the free vibrations of a simply supported TBB under different initial conditions. In this paper, the completely simplified initial boundary value problem given in the aforementioned section is solved, and the response of the beam in the time domain is obtained. The linear fundamental mode shape considering torsion angle is the initial torsional rotations $\bar{\theta}_{x0}(x)$ and the initial torsional velocities $\dot{\bar{\theta}}_{x0}(x)$ is zero. The normalization of the mode shape is achieved by specifying the amplitude of the torsion angle at the midpoint of TBB.

The time histories of the axial stress resultant $N(0,t)$ at the left end of TBB and the axial displacement $u_m(l,t)$ at the right end of TBB are presented in four cases. Obviously, the axial stress of the response over time could only be estimated through the complete initial boundary value problem, and the difference between the extreme value and the initial extreme value is significant. From this, it is pointed out that the inertia term has a certain influence on the axial stress, and it can be proved from **Figures 8–11** that its influence on the kinematical component can be ignored.

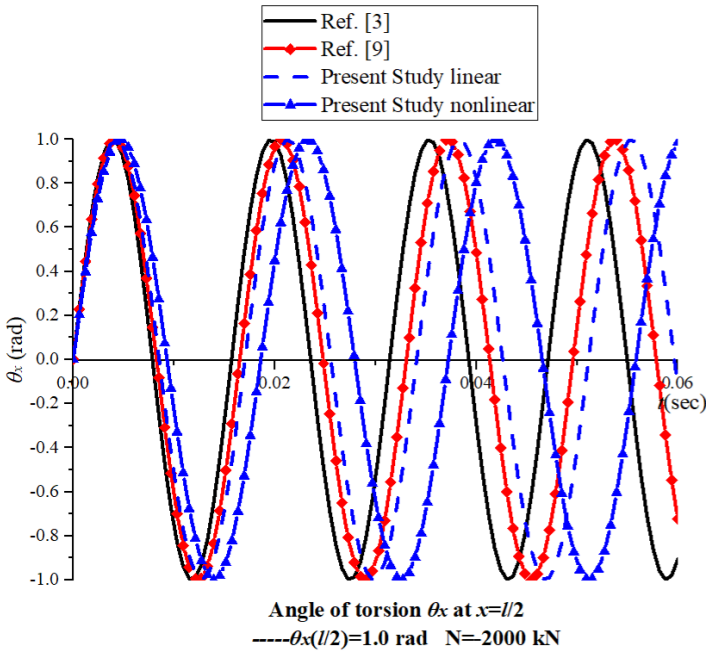

Figure 8. Time histories of the angle of torsion at the midpoint of the thin-walled box beam, for the case of initial torsional rotation $\bar{\theta}_{x0}(x)$ and initial axial displacements $\bar{u}_{x0}(x)$.

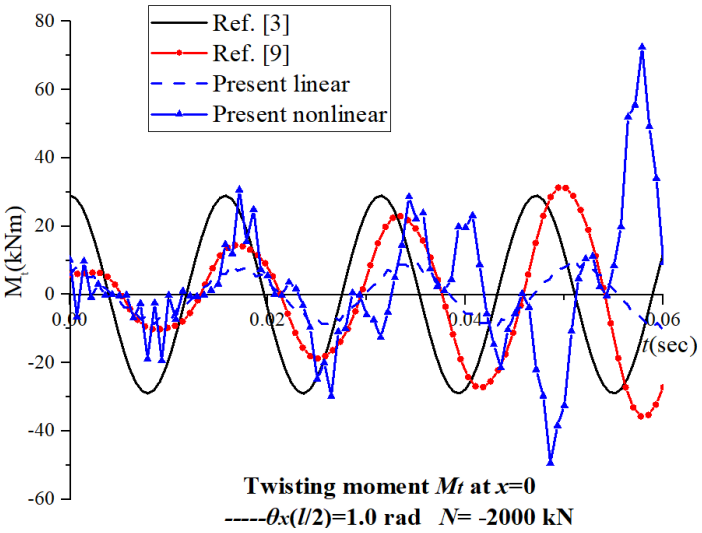

Figure 9. Time histories of the torsional moment for the case of initial torsional rotation θ_{x0} = 0.2 rad.

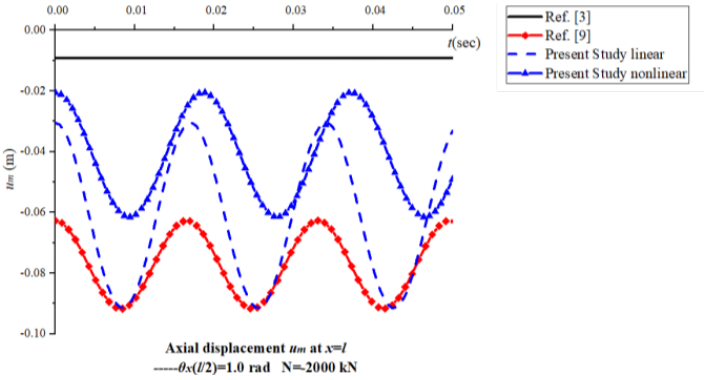

Figure 10. Time histories of axial displacement at the midpoint of the thin-walled box beam, for the case of initial torsional rotation $\bar{\theta}_{x0}(x)$.

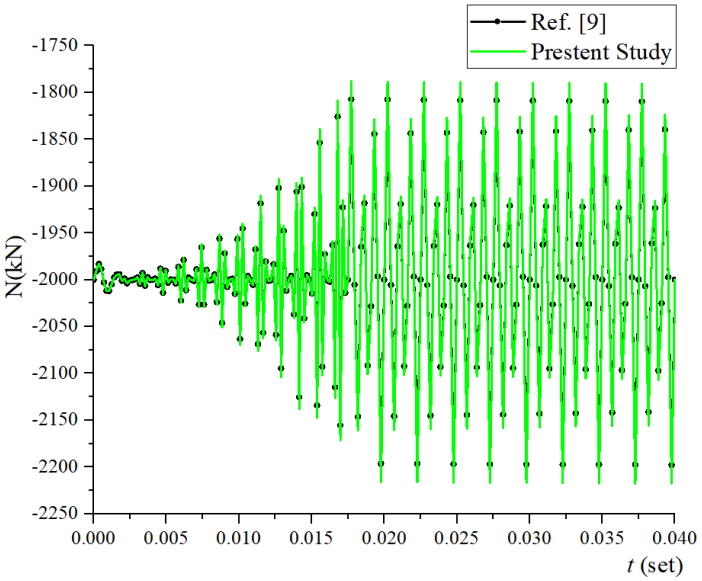

Figure 11. Time histories of axial stress resultant at the midpoint of the thin-walled box beam, for the case of initial torsional rotation $\bar{\theta}_{x0}(x)$.

In addition, it can be seen that the frequency of the axial displacement response

is almost twice that of the torsional rotation response. For the significant differences between nonlinear models and linear models, it is found that they are mainly caused by the coupling nonlinear terms of torsion, secondary torsion and distortion. The differences between the nonlinear results in Sapountzakis and Dikaros [9] and those in this paper is mainly caused by the distortion effect. The distortion and the secondary torsion effect will affect the buckling and post-buckling of the TBB, which is of good significance for the budget of the bearing capacity of the structure.

Furthermore, it can be known that the frequency of the axial displacement response is approximately twice that of the torsional rotation response. Finally, **Figure 9** shows the time history of the bending moment $M_t(0,t)$ at the left end of TBB under the above analysis, as well as the time-dependent effect of the axial inertia term on the above stress results.

5. Conclusion

In this paper, a boundary element method for nonuniform torsional vibration of TBB is established by considering the influence of distortion and geometric nonlinearty. The main conclusions come out of this survey.

(a) The numerical techniques proposed in this study are highly suitable for the computer-aided analysis of TBBs, which are supported by the most common boundary conditions and subjected to the combined action of concentrated or arbitrarily distributed axial and torsional loads that vary over time.
(b) The geometric nonlinear coupling has emerged among the torsion, distortion and axial balance equations. In addition, the resulting nonlinear term changes the modal shapes of the free vibration.
(c) Large torsional rotations add the torsional stiffness of TBB, ultimately causing a higher natural frequencies. In addition, in the special case of axial boundary conditions, the thin-walled box beam will also produce axial tensile force, resulting in the previous effects.
(d) The nonlinear coupling term produced by distortion, torsion and nonuniform torsion will affect the vibration of TBB, indicating that the distortion of TBB can not be ignored.
(e) In the analyzed examples, the axial inertia term particularly affects the axial stress resultants, while its effect on the kinematical components can be ignored.

Author contributions: MT: methodology; BL: software; YL: validation; DG: supervision. All authors have read and agreed to the published version of the manuscript.

Funding: This research was funded by Program of China Scholarship Council, grant number 202508510127, Sichuan Science and Technology Program, grant number 24ZDYF1437, Sichuan Science and Technology Program, grant number 2023YFN0009, Xizang Science and Technology Department Project, grant number XZ202401ZY00018.

Institutional review board statement: Not applicable.

Informed consent statement: Not applicable.

Data availability statement: All data generated or analysed during this study are included in this published article.

Acknowledgment: We acknowledge the support received from Program of China Scholarship Council (202508510127). In addition, Minyao Tan wants to thank, in particular, the patience,care and support from Dequan Guo the passed years.

Conflict of interest: No conflict of interest exits in the submission of this manuscript, and manuscript is approved by all authors for publication.

References

1. Rozmarynowski B, Szymczak C. Non-linear free torsional vibrations of thin-walled beams with bisymmetric cross-section. Journal of Sound and Vibration. 1984; 97(1): 145–152. doi: 10.1016/0022-460X(84)90475-9
2. Ladevèze P, Simmonds J. New concepts for linear beam theory with arbitrary geometry and loading. European Journal of Mechanics - A/Solids. 1998; 17(3): 377–402. doi: 10.1016/S0997-7538(98)80051-X
3. ADINA R&D, Inc. Theory and Modelling Guided, Volume I. ADINA R&D, Inc; 2009.
4. Przemieniecki JS. Theory of Matrix Structural Analysis. McGraw-Hill Book Co; 1968.
5. Bathe K, Chaudhary A. On the displacement formulation of torsion of shafts with rectangular cross-sections. International Journal for Numerical Methods in Engineering. 1982; 18(10): 1565–1568. doi: 10.1002/nme.1620181010
6. Sapountzakis EJ, Tsipiras VJ, Argyridi AK. Torsional vibration analysis of bars including secondary torsional shear deformation effect by the boundary element method. Journal of Sound and Vibration. 2015; 355: 208–231. doi: 10.1016/j.jsv.2015.04.032
7. Sapountzakis EJ, Mokos VG. Dynamic analysis of 3-D beam elements including warping and shear deformation effects. International Journal of Solids and Structures. 2006; 43(22–23): 6707–6726. doi: 10.1016/j.ijsolstr.2006.02.004
8. Sapountzakis EJ, Tsipiras VJ. Nonlinear nonuniform torsional vibrations of bars by the boundary element method. Journal of Sound and Vibration. 2010; 329(10): 1853–1874. doi: 10.1016/j.jsv.2009.11.035
9. Sapountzakis EJ, Dikaros IC. Non-linear flexural–torsional dynamic analysis of beams of arbitrary cross section by BEM. International Journal of Non-Linear Mechanics. 2011; 46(5): 782–794. doi: 10.1016/j.ijnonlinmec.2011.02.012
10. Sina SA, Haddadpour H, Navazi HM. Nonlinear free vibrations of thin-walled beams in torsion. Acta Mechanica. 2012; 223(10): 2135–2151. doi: 10.1007/s00707-012-0688-y
11. Sina SA, Haddadpour H. Axial–torsional vibrations of rotating pretwisted thin walled composite beams. International Journal of Mechanical Sciences. 2014; 80: 93–101. doi: 10.1016/j.ijmecsci.2013.12.018
12. Lee SJ, Park KS. Vibrations of Timoshenko beams with isogeometric approach. Applied Mathematical Modelling. 2013; 37(22): 9174–9190. doi: 10.1016/j.apm.2013.04.034
13. Stoykov S, Ribeiro P. Non-linear vibrations of beams with non-symmetrical cross sections. International Journal of Non-Linear Mechanics. 2013; 55: 153–169. doi: 10.1016/j.ijnonlinmec.2013.04.015
14. Ferradi MK, Cespedes X. A new beam element with transversal and warping eigenmodes. Computers & Structures. 2014; 131: 12–33. doi: 10.1016/j.compstruc.2013.10.001
15. Yoon K, Lee P-S, Kim D-N. Geometrically nonlinear finite element analysis of functionally graded 3D beams considering warping effects. Composite Structures. 2015; 132: 1231–1247. doi: 10.1016/j.compstruct.2015.07.024
16. Moaveni S. Finite Element Analysis: Theory and Application with ANSYS, 5th ed. Publishing House of Electronics Industry; 2021.
17. Murin J, Goga V, Aminbaghai M, et al. Measurement and modelling of torsional warping free vibrations of beams with rectangular hollow cross-sections. Engineering Structures. 2017; 136: 68–76. doi: 10.1016/j.engstruct.2016.12.037
18. Campo-Rumoroso I, Ramos-Gutiérrez ÓR, Cambronero-Barrientos F. Distortion analysis of horizontally curved trapezoidal box girder bridges. Engineering Structures. 2023; 282: 115798. doi: 10.1016/j.engstruct.2023.115798
19. Pavazza R, Matoković A, Vukasović M. A theory of torsion of thin-walled beams of arbitrary open sections

with influence of shear. Mechanics Based Design of Structures and Machines. 2022; 50(1): 206–241. doi: 10.1080/15397734.2020.1714449
20. Wang C, Wang Y. Influence of distortion ratio on distortion-induced fatigue behavior of steel girder bridges. Thin-Walled Structures. 2023; 188: 110790. doi: 10.1016/j.tws.2023.110790
21. Wang C, Wu Y, Zhang Y, et al. Distortion Effect on the UHPC Box Girder with Vertical Webs: Theoretical Analysis and Case Study. Materials. 2024; 17(6): 1303. doi: 10.3390/ma17061303
22. Wang C, Shi M, Huang J, et al. An innovative deformation coordination method for analyzing distortion effects on box girders. Scientific Reports. 2024; 14(1): 19854. doi: 10.1038/s41598-024-69130-y
23. Dikaros IC, Sapountzakis EJ, Argyridi AK. Generalized warping effect in the dynamic analysis of beams of arbitrary cross section. Journal of Sound and Vibration. 2016; 369: 119–146. doi: 10.1016/j.jsv.2016.01.022
24. Sapountzakis EJ. Torsional vibrations of composite bars of variable cross-section by BEM. Computer Methods in Applied Mechanics and Engineering. 2005; 194(18–20): 2127–2145. doi: 10.1016/j.cma.2004.07.021
25. Argyridi AK, Sapountzakis EJ. Advanced analysis of arbitrarily shaped axially loaded beams including axial warping and distortion. Thin-Walled Structures. 2019; 134: 127–147. doi: 10.1016/j.tws.2018.08.019
26. Balch CD, Steele CR. Asymptotic Solutions for Warping and Distortion of Thin-Walled Box Beams. Journal of Applied Mechanics. 1987; 54(1): 165–173. doi: 10.1115/1.3172953
27. Boswell LF, Li Q. Consideration of the relationships between torsion, distortion and warping of thin-walled beams. Thin-Walled Structures. 1995; 21(2): 147–161. doi: 10.1016/0263-8231(94)00030-4
28. Wang Z. Optimization methods for the distortion of thin-walled box girders and investigation of distortion effects. Scientific Reports. 2023; 13(1): 19166. doi: 10.1038/s41598-023-46478-1
29. Tan M, Cheng W. Non-linear lateral buckling analysis of unequal thickness thin-walled box beam under an eccentric load. Thin-Walled Structures. 2019; 139: 77–90. doi: 10.1016/j.tws.2019.02.028
30. Tan M, Guo D, Yang Q, et al. In-plane and out-of-plane free vibration analysis of thin-walled box beams based on one-dimensional higher-order beam theory. Mechanics of Advanced Materials and Structures. 2024; 31(22): 5638–5652. doi: 10.1080/15376494.2023.2218049
31. Saoula A, Meftah SA. Effect of Shear and Distortion Deformations on Lateral Buckling Resistance of Box Elements in the Framework of Eurocode 3. International Journal of Steel Structures. 2019; 19(4): 1302–1316. doi: 10.1007/s13296-019-00211-9
32. Cambronero-Barrientos F, Díaz-del-Valle J, Martínez-Martínez J-A. Beam element for thin-walled beams with torsion, distortion, and shear lag. Engineering Structures. 2017; 143: 571–588. doi: 10.1016/j.engstruct.2017.04.020
33. Arici M, Granata MF, Longo G. Symplectic analysis of thin-walled curved box girders with torsion, distortion and shear lag warping effects. Thin-Walled Structures. 2022; 175: 109244. doi: 10.1016/j.tws.2022.109244
34. Li X, Li L, Zhou M, et al. Refined beam finite element model for thin-walled multi-cell box girders considering distortion and secondary distortional moment deformation effect. Engineering Structures. 2024; 298: 117042. doi: 10.1016/j.engstruct.2023.117042
35. Fan Y-H, She G-L. Nonlinear transient response of graphene platelets reinforced metal foams beam considering initial geometrical imperfection and viscoelastic elastic foundation. Computers and Concrete. 2025; 35(1): 59–70. doi: 10.12989/CAC.2025.35.1.059
36. Zhao Y, Yuan K, Qin B, et al. A fast polynomial-FE method for the vibration of the composite laminate quadrilateral plates and shells based on the segmentation strategy. Composite Structures. 2024; 338: 118035. doi: 10.1016/j.compstruct.2024.118035
37. Zhao Y, Wang Z, Yang Z, et al. A unified hybrid Ritz-SEA acoustic vibration coupling method of a rectangular plate coupled with fast multipole boundary integration. Composite Structures. 2024; 328: 117650. doi: 10.1016/j.compstruct.2023.117650
38. Mokos VG, Sapountzakis EJ. Secondary torsional moment deformation effect by BEM. International Journal of Mechanical Sciences. 2011; 53(10): 897–909. doi: 10.1016/j.ijmecsci.2011.08.001

Appendix A. Kernels

$$\Lambda_1(r) = -\frac{1}{2}\operatorname{sgn}\rho \tag{A1}$$

$$\Lambda_2(r) = -\frac{1}{2}l(1-\rho) \tag{A2}$$

$$\Lambda_3(r) = -\frac{1}{4}l^2|\rho|(|\rho|-2) \tag{A3}$$

$$\Lambda_4(r) = -\frac{1}{12}l^3(2+|\rho|^3-3|\rho|^2) \tag{A4}$$

Appendix B

Discretization of Equations(34) and (38) and application to the *L* collocation nodal points yields:

$$\mathbf{M} = \begin{bmatrix} \rho A \cdot \mathbf{H}_1^0 & \mathbf{0} & \mathbf{0} \\ \mathbf{0} & \rho I_p \cdot \mathbf{H}_2^0 - \rho C_s \cdot \mathbf{H}_2^2 & \mathbf{0} \\ \mathbf{0} & \mathbf{0} & \rho I_q \cdot \mathbf{H}_3^0 \end{bmatrix} \tag{A5}$$

$$\mathbf{K} = \begin{bmatrix} \mathbf{F}_1 & \mathbf{E}_{12} & \mathbf{E}_{12} & & & & & & & & \\ & \mathbf{D}_{22} & \mathbf{D}_{23} & & & & & & & & \\ & & & \mathbf{F}_3 & \mathbf{E}_{35} & \mathbf{E}_{36} & \mathbf{E}_{37} & \mathbf{E}_{38} & & & \\ & & & & \mathbf{D}_{45} & \mathbf{D}_{46} & \mathbf{D}_{47} & \mathbf{D}_{48} & & & \\ & & & & & & & \mathbf{F}_5 & \mathbf{E}_{59} & \mathbf{E}_{510} & \mathbf{E}_{511} \\ & & & & & & & & \mathbf{D}_{69} & \mathbf{D}_{610} & \mathbf{D}_{611} \end{bmatrix} \tag{A6}$$

$$\mathbf{k}^{nl} = \begin{bmatrix} \mathbf{D}_{21}^{nl} & \mathbf{D}_{22}^{nl} & \mathbf{D}_{23}^{nl} & & & & & \\ & & & \mathbf{D}_{43}^{nl} & \mathbf{D}_{44}^{nl} & \mathbf{D}_{45}^{nl} & & \\ & & & \mathbf{D}_{63}^{nl} & & & \mathbf{D}_{66}^{nl} & \mathbf{D}_{67}^{nl} \end{bmatrix} \tag{A7}$$

$$\mathbf{K} = \begin{bmatrix} -EA \cdot \mathbf{I0}_1^0 & & \\ \mathbf{0} & -GI_t \cdot \mathbf{H}_2^2 + EC_s \cdot \mathbf{I0}_2 & -GI_d \cdot \mathbf{H}_3^2 \\ & -GI_d \cdot \mathbf{H}_2^2 & -GI_q \cdot \mathbf{H}_3^2 \end{bmatrix} \tag{A8}$$

$$\mathbf{f} = \begin{Bmatrix} \mathbf{n} \\ \mathbf{m}_t + \mathbf{m}'_w \\ \mathbf{m}_\chi \end{Bmatrix} \tag{A9}$$

$$(\mathbf{k}^{\mathrm{nl}})_i = -EI_p((\mathbf{H}_2^1)_i\mathbf{d}_2)((\mathbf{H}_2^2)_i\mathbf{d}_2) \tag{A10}$$

$$(\mathbf{k}^{\mathrm{nl}})_{L+i} = -\frac{3}{2}EI_{pp}[(\mathbf{H}_2^1)_i\mathbf{d}_2]^2 \begin{bmatrix} (\mathbf{H}_2^2)_i\mathbf{d}_2) - EI_p(\mathbf{d}_1)_i((\mathbf{H}_2^1)_i\mathbf{d}_2 \\ -EI_p((\mathbf{H}_1^1)_i\mathbf{d}_1)((\mathbf{H}_2^2)_i\mathbf{d}_2) \end{bmatrix} \tag{A11}$$

Generalized nonlinear and linear stiffness matrices $\mathbf{K}_{Lr}^N$, $\mathbf{K}_r^L$ and generalized mass matrix $\mathbf{M}_r$ arising from the eigenvalue problem.

$$\mathbf{K}_r^{NL}=\begin{cases}\begin{bmatrix}-\frac{I_p}{A}\tilde{N}(\mathbf{H}_2^2)_1-\frac{3}{2}EI_n[(\mathbf{H}_2^1)_1\mathbf{d}_2]^2(\mathbf{H}_2^2)_1\\-\frac{I_p}{A}\tilde{N}(\mathbf{H}_2^2)_2-\frac{3}{2}EI_n[(\mathbf{H}_2^1)_2\mathbf{d}_2]^2(\mathbf{H}_2^2)_2\\\vdots\\-\frac{I_p}{A}\tilde{N}(\mathbf{H}_2^2)_L-\frac{3}{2}EI_n[(\mathbf{H}_2^1)_L\mathbf{d}_2]^2(\mathbf{H}_2^2)_L\end{bmatrix} & rows\quad 1,2,\ldots,L\\ \begin{bmatrix}\mathbf{0}&\mathbf{0}&\mathbf{0}&\mathbf{0}\\\mathbf{0}&\mathbf{0}&\mathbf{0}&\mathbf{0}\\\mathbf{0}&\mathbf{0}&\frac{I_p}{A}\tilde{N}\cdot\mathbf{D}_{r1}^{nl}+\frac{1}{2}EI_n\cdot\mathbf{D}_{r2}^{nl}(\hat{\mathbf{u}}_2^2)&\mathbf{0}\\\mathbf{0}&\mathbf{0}&\mathbf{0}&\mathbf{0}\end{bmatrix} & rows\quad L+1,L+2,\ldots,L+8\end{cases} \tag{A12}$$

$$\mathbf{K}_r^{L}=\begin{cases}-GI_t\cdot\mathbf{H}_2^2+EC_s\cdot\mathbf{I0} & rows\quad 1,2,\ldots,L\\ \begin{bmatrix}\mathbf{F}_3&\mathbf{E}_{35}&\mathbf{E}_{36}&\mathbf{E}_{37}&\mathbf{E}_{38}\\\mathbf{F}_4&\mathbf{0}&\mathbf{E}_{46}&\mathbf{E}_{47}&\mathbf{E}_{48}\\\mathbf{0}&\mathbf{D}_{55}&\mathbf{D}_{56}&\mathbf{0}&\mathbf{D}_{58}\\\mathbf{0}&\mathbf{0}&\mathbf{D}_{66}&\mathbf{D}_{67}&\mathbf{0}\end{bmatrix} & rows\quad L+1,L+2,\ldots,L+8\end{cases} \tag{A13}$$

$$\mathbf{M}_r=\begin{cases}\rho I_p\cdot\mathbf{H}_2^0-\rho C_s\cdot\mathbf{H}_2^2 & rows\quad 1,2,\ldots,L\\ \mathbf{0} & rows\quad L+1,L+2,\ldots,L+8\end{cases} \tag{A14}$$